Asian Journal of Chemistry; Vol. 38, No. 4 (2026), 909-920
ASIAN JOURNAL OF CHEMISTRY
https://doi.org/10.14233/ajchem.2026.35084

Hexahydroquinoline-3-carbonitrile as Sustainable Corrosion Inhibitor for Mild Steel: Electrochemical and Surface Investigations

ASHLY THOMAS[1], E.P. APARNA[1], JILLY JAMES[2], PRIYA ANTONY[3] and K.S. DEVAKY[1,*]

[1]School of Chemical Sciences, Mahatma Gandhi University, Kottayam-686560, India
[2]Department of Chemistry, Alphonsa College, Pala, Kottayam-686574, India
[3]Department of Physics, Alphonsa College, Pala, Kottayam-686574, India

*Corresponding author: E-mail: ksdevakyscsmgu@gmail.com

Received: 17 October 2025 *Accepted*: 3 February 2026 *Published online*: 8 April 2026 AJC-22312

A simple and eco-friendly microwave-assisted approach was applied to synthesise hexahydroquinoline-3-carbonitrile derivatives as corrosion inhibitors. The quinoline derivatives were obtained by reacting nitriles and chalcones with ammonium acetate under microwave irradiation. The synthesised hexahydroquinoline-3-carbonitriles were characterised using FT-IR, ^{1}H NMR, ^{13}C NMR, HRMS and SCXRD techniques. The efficiency of synthesised hexahydroquinoline-3-carbonitriles in inhibiting corrosion on mild steel was investigated using electrochemical methods (EIS and polarisation) and surface morphological analysis (AFM). According to EIS and polarization studies, hexahydroquinoline-3-carbonitriles act as mixed-type corrosion inhibitors by adsorbing at the metal/electrolyte interface and thereby preventing mild steel corrosion. The AFM analysis also confirmed that the hexahydroquinoline-3-carbonitriles were successfully adsorbed onto the surface of mild steel.

Keywords: Microwave synthesis, Quinoline derivatives, Corrosion inhibitor, Mild steel, Electrochemical impedance spectroscopy.

INTRODUCTION

Quinoline is an aromatic heterocyclic compound with the molecular formula C_9H_7N. It features a bicyclic structure, formed by the fusion of a pyridine ring with a benzene ring at two neighbouring carbon atoms. In addition to being employed as starting materials in the synthesis of alkaloids and fungicides, quinoline derivatives are highly valuable in the fields of medicine, catalysts, food, dye, refineries, electronics, *etc*. [1,2]. Moreover, quinolines are very useful synthons that are used to create polymers and nanostructures that have outstanding mechanical properties along with excellent electrical, photonic and nonlinear optical capabilities [3,4]. Quinoline-based compounds play a significant role in everyday applications, including dyes, food colourants, pH indicators and other chemical substances [5].

Corrosion is a process by which metals undergo deterioration because of the chemical contact with the environment. Both direct and indirect corrosion seem to be responsible for the loss of a vast amount of metal on a global scale. Due to its high mechanical strength, ease of fabrication and affordability, mild steel, a low carbon steel alloy, is used extensively as a building material in a wide range of industries, including the food, energy and chemical sectors. Mild steel, though widely used, is highly susceptible to corrosion. In aggressive or acidic environments, it tends to deteriorate rapidly, especially during industrial operations like acid pickling, descaling, etching, cleaning and oil well acid treatment [6,7].

The various techniques usually adopted to prevent or control the corrosion of metals are metallic and non-metallic protective coating, cathodic protection, anodic protection, alloying of metals and the amendment of the corrosive environment using inhibitors [8-10]. Corrosion inhibitors will minimize the cost of both or each of anodic oxidation and cathodic reduction. The ability of organic, inorganic and polymer materials to prevent corrosion in acidic solutions has been widely investigated [11-13]. The acetylenic alcohols, alkenylphenones, aromatic aldehydes, nitrogen containing heterocycles and their quaternary salts and condensation products of carbonyl compounds are generally found as effective acidizing inhibitors [14-16]. Among the N-heterocyclic compounds, acetylenic alcohols adsorb and often polymerize on

the steel surface at high temperatures, forming a more thermally stable, adherent barrier film during acidizing, whereas carbonitriles, in contrast, inhibit corrosion mainly by donating the nitrogen lone pair (and π-electrons of the C≡N group) to iron, forming a strongly adsorbed protective film that blocks acid attack. Quinoline derivatives, like carbonitriles, donate the nitrogen lone pair to iron, but their fused aromatic system increases the π-electron density, enhancing adsorption and forming a more compact, stable protective film in acidic media.

This study explores the ability of quinoline derivatives containing carbonitrile group to protect mild steel from corrosion in acidic environments through an adsorption-based mechanism. Their corrosion inhibition performance was assessed using Tafel polarization and electrochemical impedance spectroscopy (EIS). To support the electrochemical findings, atomic force microscopy (AFM) was also employed to examine the steel surface before and after immersion in the corrosive medium.

EXPERIMENTAL

The chemicals, reagents and solvents including 3-aminocrotonitrile, aldehydes, ketones, ethyl cyanoacetate and malononitrile were procured from Spectrochem Chemicals Pvt. Ltd. India; Thermo Scientific Chemicals, U.K.; and Merck, USA. The other reagents and solvents used were obtained from the local suppliers and were purified in accordance with typical procedures before use.

Characterisation: The Fourier transform infrared (FT-IR) spectra were obtained using a Perkin-Elmer 400 FT-IR spectrophotometer. ^{1}H NMR and ^{13}C NMR spectra of the samples were measured from Bruker Advance DPX-300 MHz FT-NMR spectrometer (400 MHz) in DMSO-d_6/$CDCl_3$. The mass spectra were recorded using LC-Q-ToF (Xevo, G2Q-ToF MS System, Waters) and LC-MS/MS (Shimadzu 8045). Single crystal data collections were done using Bruker Kappa AXS Diffractometer. Hirshfeld surface analysis and the concomitant two-dimensional fingerprint plots recorded using the program CrystalExplorer17.5. The electrochemical studies were carried out by means of a CH electrochemical workstations model CHI608 E. Atomic force micrographs (AFM) were recorded using WITec Alpha 300RA AFM & Raman instrument (WITec-GmbH, Germany). A microwave synthesizer (Anton Paar, Monowave 300) was used to perform the microwave assisted synthesis.

Microwave assisted synthesis of hexahydroquinoline-3-carbonitriles (56a-f)

Synthesis of substituted 2-benzylidene cyclohexane-1,3-diones: 2-Benzylidenecyclohexane-1,3-dione derivatives **53** were synthesized *via* Claisen-Schmidt reaction by reacting cyclohexane-1,3-dione (**50**) with substituted benzaldehydes (**51**) in alkaline ethanolic medium at room temperature, as illustrated in **Scheme-I**. Once the reaction was completed, the precipitated cyclic chalcone was separated by filtration and washed with cold water. To enhance purity, the crude chalcones were subjected to recrystallisation in absolute ethanol. The chalcones were obtained in 55-80% yields.

Synthesis of hexahydroquinoline-3-carbonitriles (56a-f): The quinoline derivatives **56a-f** were obtained by reacting nitriles with the synthesised chalcones (**53a-c**) in the presence of ammonium acetate. The reaction was carried out in absolute ethanol under microwave irradiation at 140 ºC for 30 min (**Scheme-I**). The products formed were separated by column

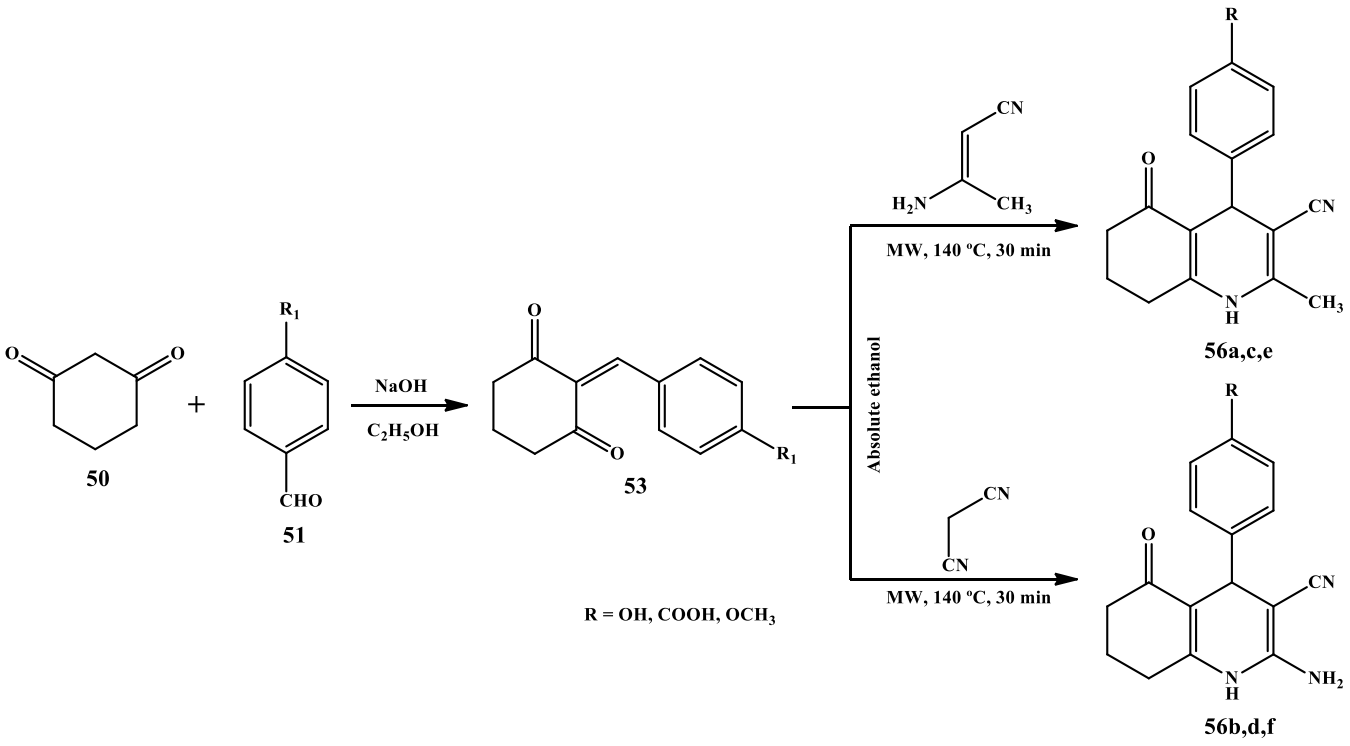

Scheme-I: Microwave mediated synthesis of quinoline-3-carbonitriles

chromatography over silica gel using hexane/ethyl acetate mixture.

2-Methyl-4-(4-hydroxyphenyl)-5-oxo-1,4,5,6,7,8-hexahydroquinoline-3-carbonitrile (56a): Yield: 70%; FTIR (KBr, ν_{max}, cm^{-1}): 3232 (OH), 3128 (NH), 3022 (Ar C-H), 2935 (alkyl C-H), 2204 (C≡N), 1661 (C=O); ^{1}H NMR (DMSO-d_6 δ ppm): 9.45 (s, 1H, OH), 2.03 (s, 3H, CH_3), 4.30 (s, 1H, C8 H, quinoline ring), 6.63-6.95 (4H, Ar-H), 9.26 (s, 1H, NH), 2.50 (2H, C11 H), 1.88 (2H, C12 H), 2.16 (2H, C13 H); ^{13}C NMR (DMSO-d_6 δ ppm): 115.2 (C≡N), 194.4 (C=O), 17.5 (CH_3), 151.2, 145.5, 108.9, 86.0, 36.9, (C, quinoline ring), 36.5, 26.0, 20.6, (alkyl-C, quinoline ring), 155.8, 136.5, 128.0, 119.9 (Ar, C); LC-Q-ToF MS: 279.4835 [M-1]; Elemental analysis of $C_{17}H_{16}N_2O_2$: calcd. (found) %: C, 72.84 (72.61); H, 5.75 (6.10); N, 9.99 (10.11).

2-Amino-4-(4-hydroxyphenyl)-5-oxo-1,4,5,6,7,8-hexahydroquinoline-3-carbonitrile (56b): Yield: 68%; FTIR (KBr, ν_{max}, cm^{-1}): 3429 (OH), 3293-3232 (NH_2), 3108 (NH), 3004 (Ar C-H), 2815 (alkyl C-H), 2204 (C≡N), 1663 (C=O); ^{1}H NMR (DMSO-d_6 δ ppm): 3.36 (s, 1H, C8H, quinoline ring), 6.43-7.61 (4H, ArH), 7.22 (d, 2H, NH_2), 9.98 (1H, NH), 2.05 (2H, C11H), 1.74 (2H, C12H), 1.92 (2H, C13H); ^{13}C NMR (DMSO-d_6 δ ppm): 112.2 (C≡N), 197.8 (C=O), 159.1, 149.2, 123.2, 89.2, 39.5 (C, quinoline ring), 29.1, 23.6, 20.8 (Alkyl C, quinoline ring), 154.1, 139.4, 131.8, 131.2, 118.6, 117.7 (Ar, C); MS/MS: 281; Elemental analysis of $C_{16}H_{15}N_3O_2$: calcd. (found) %: C, 68.31 (68.02); H, 5.37 (5.51); N, 14.94 (14.63)

2-Methyl-4-(4-carboxylphenyl)-5-oxo-1,4,5,6,7,8-hexahydroquinoline-3-carbonitrile (56c): Yield: 61%; FTIR (KBr, ν_{max}, cm^{-1}): 3312 (NH), 3078 (Ar C-H), 2654 (alkyl C-H), 2208 (C≡N), 1658, 1636 (C=O); ^{1}H NMR (DMSO-d_6 δ ppm): 12.41 (s, 1H, COOH), 2.28 (s, 3H, CH_3), 4.24 (s, 1H, C8H, quinoline ring), 6.91-7.49 (4×ArH), 9.20 (s, 1H, NH); 1.88 (2H, C11-H), 1.56 (2H, C12H), 1.67 (2H, C13H); ^{13}C NMR (DMSO-d_6 δ ppm): 115.0 (C≡N), 119.7 (CH_3), 169.5 (COOH),196.1 (C=O), 167.1, 165.1, 120.4, 66.8, 91.2 (C, quinoline ring), 26.2, 31.0, 36.0 (alkyl-C, quinoline ring), 149.3, 129.4, 128.1, 128.7, 128.8, (Ar, C); LC-Q-ToF MS: 308.1038; Elemental analysis of $C_{18}H_{16}N_2O_3$: calcd. (found) %: C, 70.12 (70.82); H, 5.23 (5.90); N, 9.09 (9.18).

2-Amino-4-(4-carboxylphenyl)-5-oxo-1,4,5,6,7,8-hexahydroquinoline-3-carbonitrile (56d): Yield: 75%; FTIR (KBr, ν_{max}, cm^{-1}): 3459 (OH), 3319 (NH_2), 3184 (NH), 2915 (Ar C-H), 2879 (alkyl C-H), 2182 (C≡N), 1680, 1667 (C=O); ^{1}H NMR (DMSO-d_6 δ ppm): 4.50 (s, 1H, C8H, quinoline ring), 7.01-7.86 (4H, ArH), 6.15 (2H, NH 2), 9.59 (1H, NH); 2.48 (2H, C11H), 1.75 (2H, C12H); 2.18 (2H, C13H); ^{13}C NMR (DMSO-d_6 δ ppm): 196.3 (C=O), 116.8 (C≡N), 168.7 (COOH), 153.7, 151.8, 109.6, 87.0, 39.5 (C, quinoline ring), 28.1, 21.9, 19.4 (alkyl-C, quinoline ring), 148.0, 131.1, 130.7, 129.8, 128.6, 128.4 (Ar, C); MS/MS: 309; Elemental analysis of $C_{17}H_{15}N_3O_3$: calcd. (found) %: C, 66.01 (65.82); H, 4.89 (5.13); N, 13.58 (14.17).

2-Methyl-4-(4-methoxyphenyl)-5-oxo-1,4,5,6,7,8-hexahydroquinoline-3-carbonitrile (56e): Yield: 82%; FTIR (KBr, ν_{max}, cm^{-1}): 3195 (NH), 3080 (Ar C-H), 2955 (alkyl C-H), 2197 (C≡N), 1600 (C= O); ^{1}H NMR (DMSO-d_6 δ ppm): 3.47 (s, 3H, OCH_3), 3.31 (s, 3H, CH_3), 3.98 (s, 1H, C8H, quinoline ring), 6.43-7.49 (4H, ArH), 9.48 (1H, NH), 2.09 (2H, C11H), 1.50 (2H, C12H), 1.79 (2H, C13H); ^{13}C NMR (DMSO-d_6 δ ppm): 56.1 (OCH_3), 115.0 (C≡N), 194.9 (C=O), 18.0 (CH_3), 152.0, 146.3, 109.4, 86.8, 55.4 (C, quinoline ring), 37.1, 26.4, 21.1 (alkyl-C, quinoline ring), 158.2, 138.5, 132.2, 128.5, 120.3, 114.1 (Ar C); LC-Q-ToF MS: 293.1573 [M-1]. Elemental analysis of $C_{18}H_{18}N_2O_2$: calcd. (found) %: C, 73.45 (73.62); H, 6.16 (6.38); N, 9.52 (9.77).

2-Amino-4-(4-methoxyphenyl)-5-oxo-1,4,5,6,7,8-hexahydroquinoline-3-carbonitrile (56f): Yield: 81%; FTIR (KBr, ν_{max}, cm^{-1}): 3330 (NH_2), 3029 (Ar C-H), 2932 (alkyl C-H), 2228 (C≡N), 1681 (C=O), 1277, 1020 (C-O-C, methoxy group); ^{1}H NMR (DMSO-d_6 δ ppm): 3.66 (s, 3H, OCH_3), 3.87 (s, 1H, C8H, quinoline ring), 6.69-7.09 (4H, ArH), 6.89 (2H, NH_2), 2.42 (2H, C11H), 1.85 (2H, C12H); 2.15 (2H, C13-H); ^{13}C NMR (DMSO-d_6 δ ppm): 54.4 (OCH_3), 115.4 (C≡N), 195.3 (C=O), 36.4, 59.7, 100.4, 156.5, 166.9 (C, quinoline ring), 31.0, 20.1, 28.2 (alkyl-C, quinoline ring), 156.4, 112.1, 128.2, 128.8, 136.9 (Ar, C); LC-Q-ToF MS: 295.1894; Elemental analysis of $C_{17}H_{17}N_3O_2$: calcd. (found) %: C, 69.14 (69.64); H, 5.80 (6.04); N, 14.23 (14.19).

Corrosion inhibitory studies: All the synthesised quinoline-3-carbonitriles (**56a-f**) were studied as inhibitors for the corrosion of mild steel in 1 M HCl solution. The corrosion inhibitory studies of the samples were executed using electrochemical method such as Tafel plot and electrochemical impedance spectroscopy (EIS) measurements. Atomic force microscopy (AFM) was employed to investigate the surface morphology of mild steel specimens immersed for 3 h in 1 M HCl solution in the presence of inhibitor.

Electrode preparation: A mild steel strip sized 6 cm × 2 cm × 0.05 cm was cut from MS sheet served as the working electrode. The chemical composition of MS (wt.%) was C (11.84%), Si (0.57%), O (2.03%) and Fe (85.56%). The MS strip was covered with an insulation tape excluding its underneath surface with surface area of 1 cm^2. The surface of MS electrodes was mechanically polished prior to use with emery paper (SiC) of different grades ranging from 800-1200 grits. The MS specimen was then degreased with acetone and washed with double distilled water, followed by immediate exposure to the test solution.

Preparation of corrosive medium: The analytical grade hydrochloric acid (37% HCl) was diluted with double-distilled water to obtain a 1 M HCl solution, which served as the corrosive medium. The corrosion tests were carried out in a 1 M HCl solution with inhibitor concentrations ranging from 0.001 M to 0.15 M. A blank experiment was also carried out.

Electrochemical impedance spectroscopy (EIS) measurements: The EIS measurements were carried out over a frequency range of 0.010 Hz to 100 kHz at the open-circuit potential, following a 3 h immersion of the mild steel (MS) strip in the test solution. All the obtained EIS data were fitted with suitable equivalent circuit using software Z-Simp Win. Electrochemical impedance spectroscopy (EIS) and potentiodynamic polarisation curve measurements (Tafel plot) were carried out by means of CHI608E model electrochemical workstation, Ag/AgCl as the reference electrode, a platinum

wire as the counter electrode and mild steel coupons with surface area of 1 cm^2 as the working electrode. All of the electrochemical studies were employed after dipping the mild steel electrode in the test solution for 3 h at 27 ºC in order to establish a steady state open circuit potential (OCP). The corrosion behaviour of the mild steel specimens was investigated in 1 M HCl solution using EIS and cathodic (from open circuit potential, E_{ocp} to -0.25 V, scan rate of 0.001 V s^{-1}) and anodic (from E_{ocp} to +0.25 V scan rate of 0.001 V s^{-1}) polarisation curves in the test solution containing inhibitor. For comparison, a blank experiment was also conducted without using inhibitor.

The equivalent circuit used to fit the impedance data is shown in Fig. 1. The Randle's equivalent circuit consists of the electrolyte resistance (R_s) connected in series with a parallel network includes the charge transfer resistance (R_{ct}) and a constant phase element (CPE). The CPE was used instead of the ideal double-layer capacitance to achieve a better agreement with the experimental data.

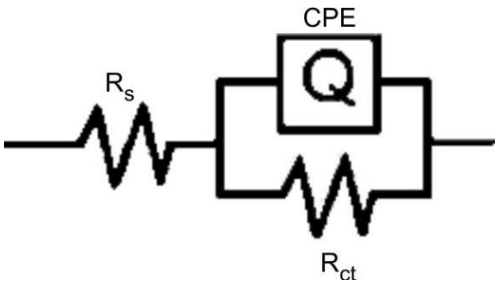

Fig. 1. Randle's equivalent circuit proposed to fit the EIS experimental data

The inhibition efficiency was calculated from polarisation measurements according to the equation given below:

$$\eta\% = \frac{I_{corr} - I_{corr(inh)}}{I_{corr}} \times 100 \quad (1)$$

where I_{corr} and $I_{corr(inh)}$ represent the uninhibited and inhibited corrosion current densities of the analysed samples.

Tafel polarisation measurements: Inhibition efficiencies were determined from corrosion currents obtained by the Tafel extrapolation method and fitting the curve to the polarisation equation. The reported procedure was followed for the polarisation measurements [17,18]. The polarisation curves were acquired potentiodynamically between -0.25 V and +0.25 V with a scan rate of 1 mV s^{-1} in 1 M HCl solution containing inhibitor. The MS electrode was immersed in the test solution for 3 h before each experiment and then the measurements were taken after attaining the balanced state of E_{ocp} (electrode open circuit potential). Linear polarisation resistance (LPR) was achieved by scanning the electrode potential ±0.010 V (Ag/AgCl) around E_{ocp} starting from more cathodic potentials to anodic direction. The scan rate was 0.001 Vs^{-1}. The polarisation resistance R_p was obtained from the slope of the potential-current figures.

Surface analysis: AFM analyses were conducted for the surface analysis. The mild steel specimens having dimensions of 1 cm × 1 cm × 0.05 cm were immersed in 1 M HCl for 3 h time in absence and presence of synthesised quinoline derivatives were used for the surface morphological studies.

RESULTS AND DISCUSSION

An eco-friendly microwave-assisted method was employed for the synthesis of hexahydroquinoline-3-carbonitrile (**56a-f**). In this, 2-aminohexahydroquinoline-3-carbonitriles **56b,d,f** were synthesised by using malononitrile while 3-aminocrotononitrile was used for 2-methyl hexahydroquinoline-3-carbo nitriles **56a,c,e**. Initially, 2-(4-methoxybenzylidene) cyclohexane-1,3-dione (**53**), malononitrile and ammonium acetate in absolute ethanol were taken as model substrates for studying the synthesis of 2-alkylhexahydroquinoline-3-carbonitrile (**56f**) under microwave irradiations. All the compounds **56a-f** were characterised by FT-IR, ^{1}H NMR, ^{13}C NMR and HRMS techniques. The molecular structure of compound **56f** was verified through single-crystal X-ray diffraction analysis. Compound **56f** was selected as the representative compound, and its detailed spectral data are discussed.

The structure of compound **56f** was confirmed by FT-IR spectroscopy, which showed characteristic absorption bands at 3330 cm^{-1} (NH_2 *str.*), 2228 cm^{-1} (CN *str.*) and 1681 cm^{-1} (C=O *str.*) (Fig. 2a). The ^{1}H NMR spectrum of compound **56f** shows a singlet at δ 3.66 ppm corresponding to the methoxy protons (3H) and a singlet at δ 3.87 ppm assigned to the methine proton at C8 (1H). A broad signal at at δ 6.89 ppm is attributed to the NH_2 protons (2H), while the aromatic protons (4H) appear as doublets in the range δ 6.69-7.09 ppm. The signals at δ 1.85, 2.15, and 2.42 ppm correspond to the alkyl CH_2 protons (6H) of the cyclohexanone ring fused to the quinoline system (Fig. 2b). The characteristic ^{13}C NMR signal due to OCH_3 carbon appeared at δ 54.43 ppm. The cyano carbon give a signal at δ 115.4 ppm and the C2, C3, C4, C5, C6, C7 carbon atoms in the phenyl ring resonated at δ values 156.4, 112.1, 128.2, 128.8 and 136.9 ppm, respectively. The carbonyl carbon gives the signal at δ 195.3 ppm. The C11, C12, C13, C8 alkyl carbon atoms in the quinoline ring show signals at δ values 31.0, 20.1, 28.2, 36.4 ppm, respectively. The signals of C9, C14, C15, C16 carbon atoms appeared at δ values 100.4, 156.5, 166.9, 59.7 ppm, respectively (Fig. 2c). Furthermore, the HRMS spectrum (Fig. 2d) showed a molecular ion peak at *m/z* 295.1894, which matches the calculated value for the molecular formula $C_{17}H_{17}N_3O_2$, thereby confirming the proposed structure of compound **56f**.

Single crystal X-ray diffraction analysis: The ORTEP representation of **56f** with all atoms represented as 50% probability ellipsoid is shown in Fig. 3 (CCDC No. 1910687). The molecule **56f** crystallizes in monoclinic crystal system with $P2_1/c$ space group. The lattice parameters are a = 8.6230 (8) Å, b = 16.7094 (13) Å, c = 10.5207 (9) Å and α = γ = 90º, β = 104.285 (4)º. The cell volume is 1469.0 (2) $Å^3$ containing Z = 4 formula units.

The single crystal X-ray diffraction studies of the colourless crystal of **56f** were accomplished successfully, showing distinct conformation behaviour of aryl groups linked to the quinoline moiety. Compound **56f** consists of a quinoline unit connected to a methoxyphenyl ring at C8, a cyano group at C16, an amino group at C15 and an oxygen atom at C10 atom. The six membered carbocyclic ring (C9–C14) of the quinoline moiety holds an envelope conformation with

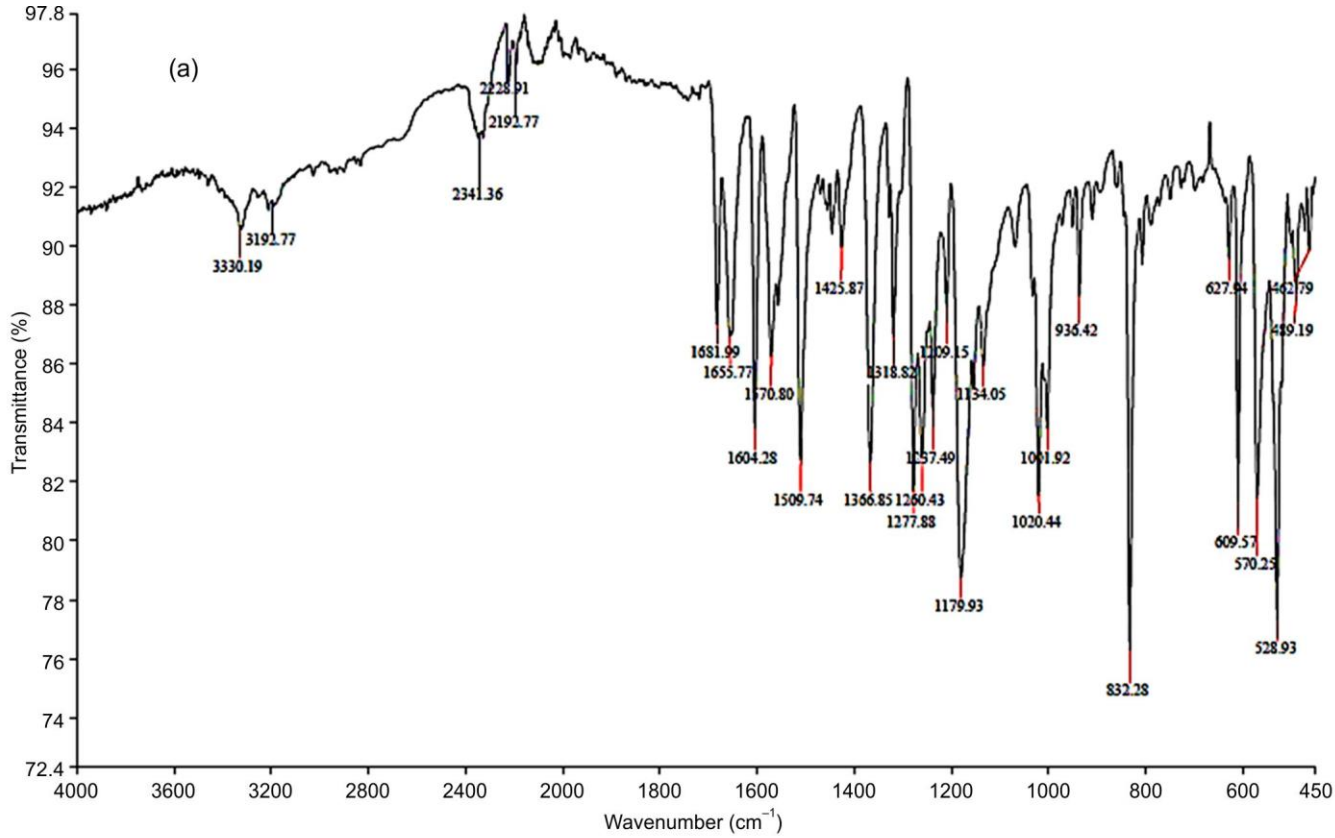
(a)
Transmittance (%)
Wavenumber (cm⁻¹)
3330.19
3192.77
2341.36
2228.91
2192.77
1681.99
1655.77
1670.80
1604.28
1509.74
1425.87
1366.85
1318.82
1277.88
1260.43
1257.49
1209.15
1179.93
1134.05
1091.92
1020.44
936.42
832.28
627.94
609.57
570.25
528.93
462.79
459.19

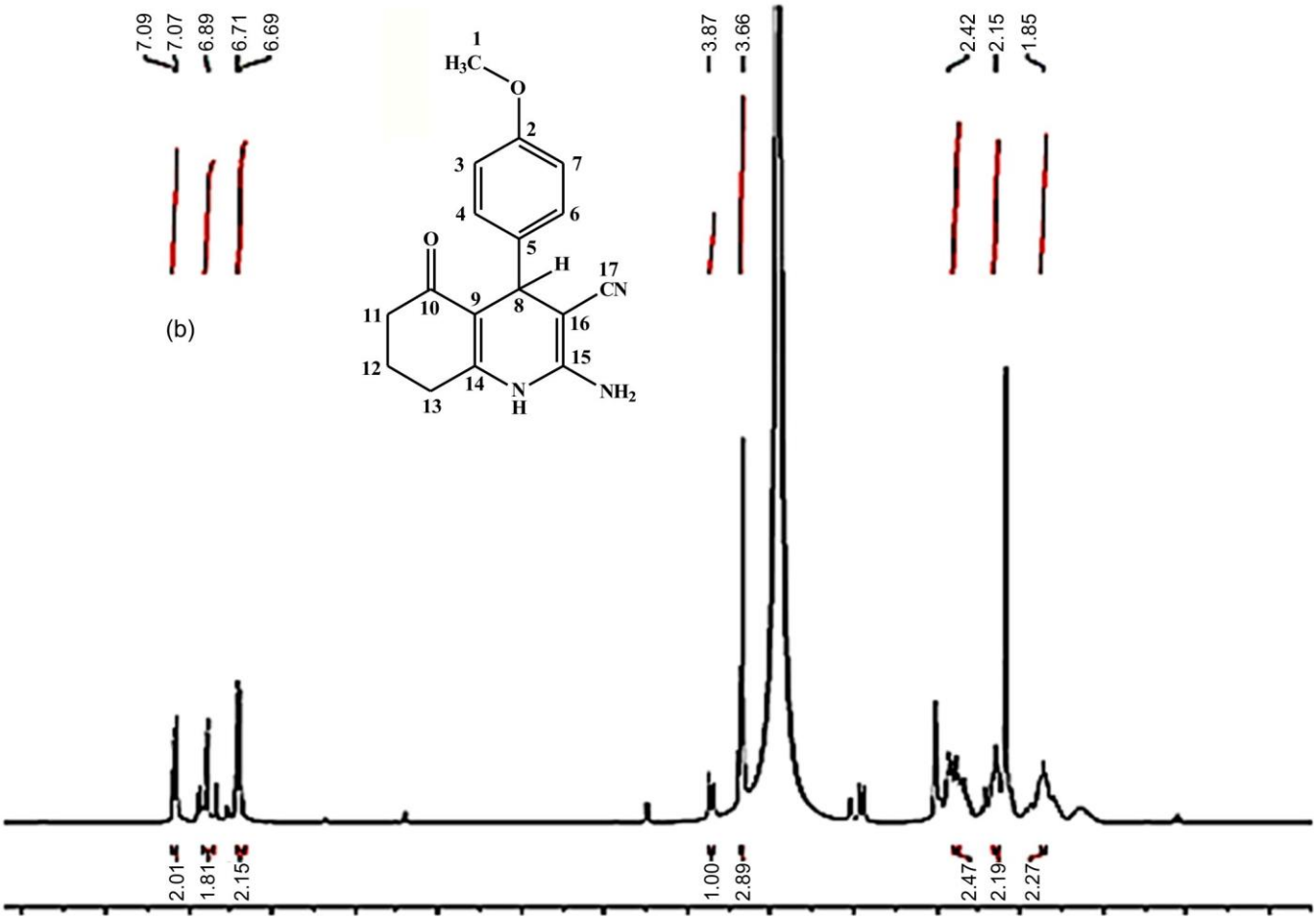
(b)
7.09
7.07
6.89
6.71
6.69
3.87
3.66
2.42
2.15
1.85
2.01
1.81
2.15
1.00
2.89
2.47
2.19
2.27
H3C
O
NH2
CN
N
H

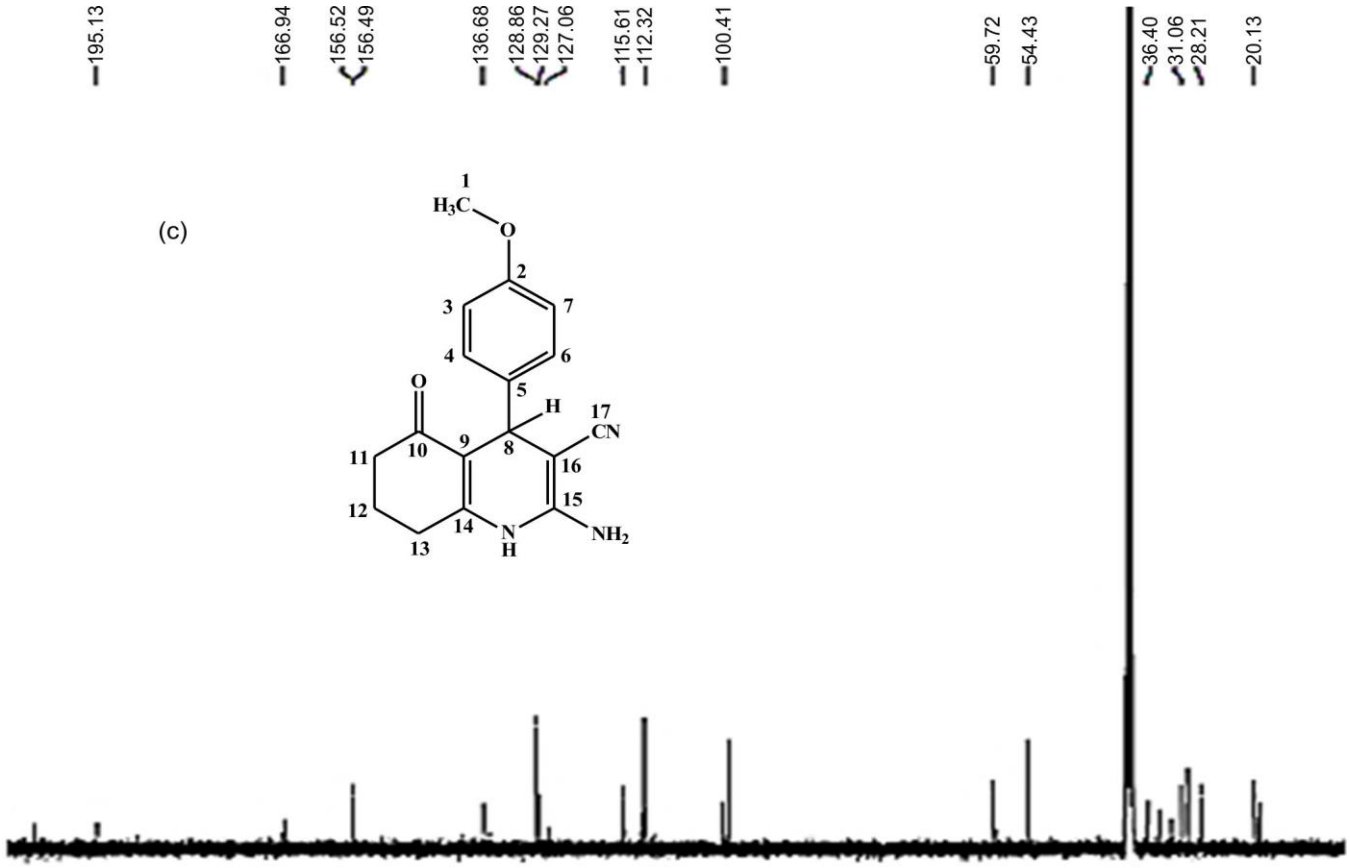

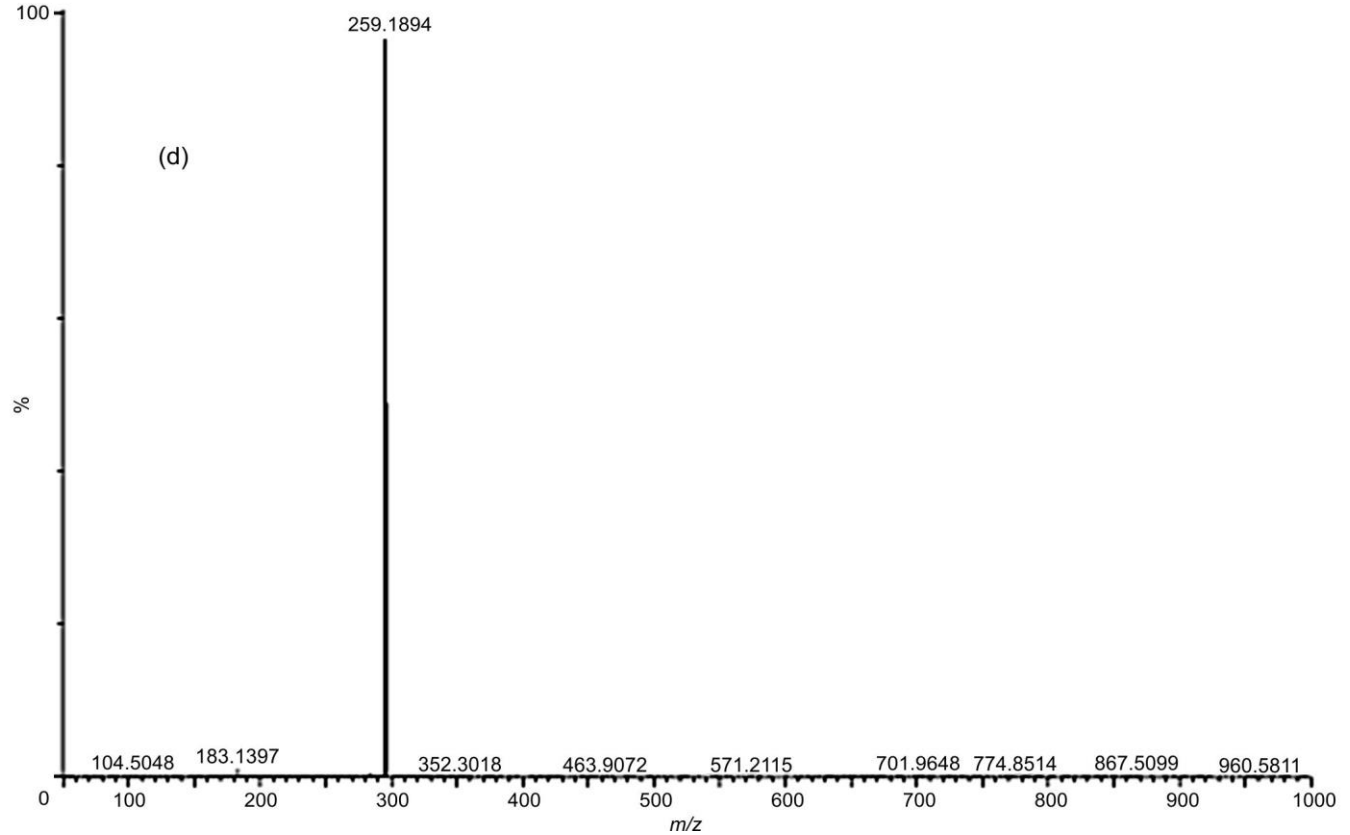

Fig. 2. (a) FT-IR, (b) ^{1}H NMR, (c) ^{13}C NMR and (d) HRMS spectra of 2-amino-4-(4-methoxyphenyl)-5-oxo-1,4,5,6,7,8-hexahydro-quinoline-3-carbonitrile (**56f**)

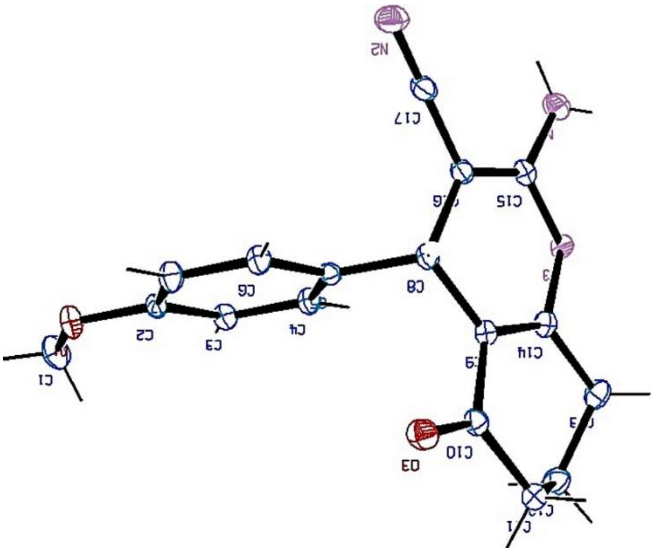

Fig. 3. ORTEP diagram of the synthesised 2-amino-4-(4-methoxyphenyl)-5-oxo-1,4,5,6,7,8-hexahydroquinoline-3-carbonitrile (**56f**)

C12 as the flap atom with puckering amplitude (Q) = 0.459 (1) Å, θ = 58.20 (1)º φ = 174.13(2)º [19]. The C12 atom deviates by 0.339 (1) Å from the mean plane passing through the remaining ring atoms.

The cyano and amino groups are coplanar with the quinoline moiety mean plane, with torsion angles N1–C15–N3–C14=173.9 (2)º and N3–C15–C16–C17= 179.6 (2)º. The quinoline unit plane (N3/C8–C16) forms a dihedral angle of 81.49 (8)º with the benzene ring C2–C7. The torsion angle for C4–C5–C8–C10 is 74.3(2)º. The non-coplanarity of the benzene ring was due to the presence of oxygen atom at the C10 carbon atom. So, the free rotation around C8–C5 bond was hindered by a steric effect of oxygen atom. For instance, bond distance measurements in the SCXRD data shows that the bond length of C9–C10 is 1.465 (3) Å, while the bond length of C9–C14 and C10–C11 are 1.336 (3) Å and 1.501 (3) Å, respectively. It displays that C9–C10 has partial double bond character, which may due to keto-enol (C=O/C–OH) equilibrium of the C=O group in the compound by the shift of proton on N3.

The molecular structure was further supported by an intermolecular N1–H1···O1 hydrogen bond, which links the molecules into corrugated layers (Fig. 4a). In the crystal packing, molecules are linked *via* pairs of C7–H7A···O3 hydrogen bonds which generate a $R_2^2(16)$ ring motif [20]. The formed dimers were connected by further C1–H1A···O3 hydrogen bonds (Fig. 4b). The molecule is also associated with N1–H1···C short contacts. The details of hydrogen bond geometry are given in Table-1.

TABLE-1
HYDROGEN BOND GEOMETRY IN **56f** (Å, º)

D–H···A	D–H	H···A	D···A	D–H···A
N1–H1N1···O1	0.88	2.06	2.9450 (3)	175
C1–H1A···O3	0.96	2.58	3.5274 (3)	167
C7–H7···O3	0.93	2.50	3.3615 (3)	155

Symmetrycodes: (i) 2-x,-y, 1-z; (ii) x,y,-1+z; (iii) -1+x,y,z

Hirshfeld surface analysis: The intermolecular interactions present in the molecule **56f** were examined through Hirshfeld surface analysis and the corresponding 2D fingerprint plots were generated using the Crystal-Explorer17 software [21]. The d_i, d_e and d_{norm}, shape index and curvedness in Hirshfeld surface were plotted over, where the d_{norm} ranges from -0.5192 to 1.4274 Å, shape index ranges from -1.0 to1.0 Å, curvedness ranges from -4.0 to 4.0 Å and d_i and d_e range from -0.7932 to 2.5184 Å, respectively. The mapping of d_i, d_e, d_{norm}, the shape index and curvedness are shown in Fig. 5.

In Fig. 5a, the bright red spots near atoms N1, O1 and hydrogen atoms H1N1, H2N1, H1A and H7 indicate their roles as hydrogen bond donors and/or acceptors. The curvedness map describes the surface shape of the molecule: broad green regions represent relatively flat areas with low curvedness, while dark blue edges indicate highly curved regions. This analysis is useful for identifying possible π-π interactions between neighbouring molecules. In Fig. 5c, the shape index of the Hirshfeld surface indicates the absence of π–π interactions in compound **56f**, as no adjacent red and blue triangular patterns are observed, which would otherwise signify close contact between aromatic rings.

Fig. 6a indicates the overall 2D fingerprint plot and Fig. 6b-e designates the delineated fingerprint plots on H···H, N···H/H···N, C···H, O···H/H···O interactions. In addition, there are other minor interactions like C···C, C···N, C···O, N···N, O···N, *etc*. (6.3%), are also involved in the molecule. These plots provide the information about the major and minor percentage contribution of interatomic contacts in the compound. The H···H interactions contribute the half of the total (46.2%) to the overall crystal packing with a sting at about $d_i = d_e = 1.8$ Å (Fig. 6b). The symmetrical pair of wings

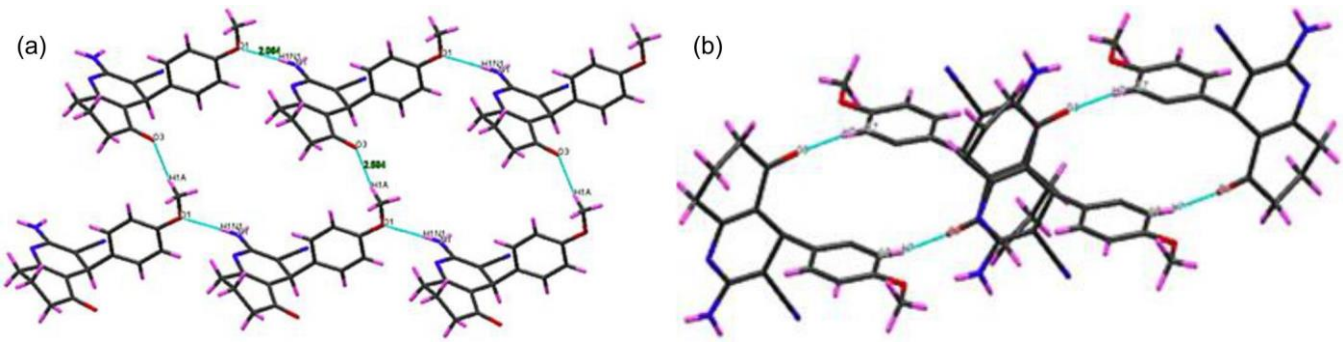

Fig. 4. (a) The chain structure of **56f** formed *via* N1–H1···O1 and C1–H1A···O3 interactions (blue dashed lines) along the *a*-axis direction, (b) A view showing the $R_2^2(16)$ ring motif built by C7–H7A···O3 hydrogen bonding

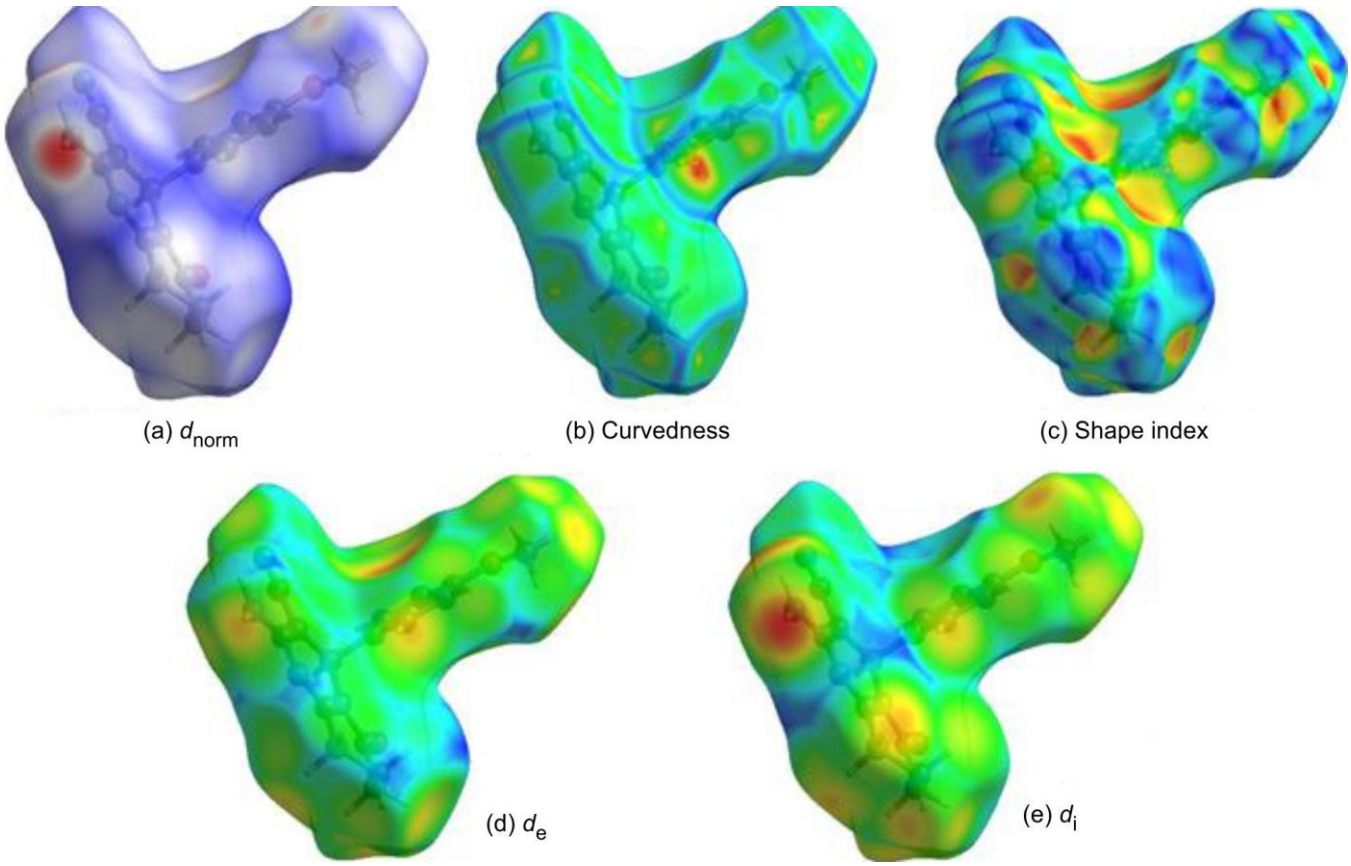

Fig. 5. The plotting of d_i, d_e, d_{norm}, shape index and curvedness of **56f**

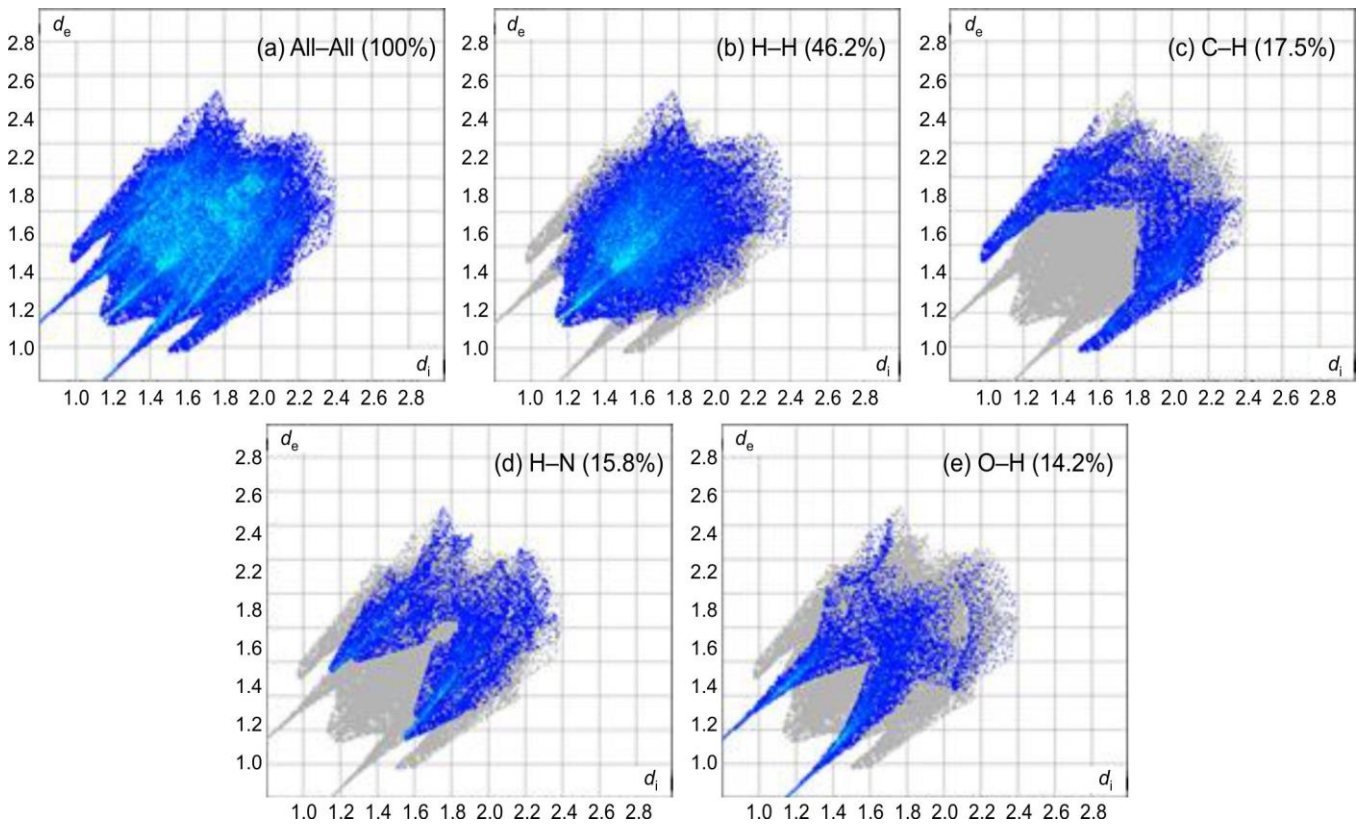

Fig. 6. 2D finger print plots of **56f**

with the tips at $d_e + d_i$ = 2.5 Å in Fig. 6c arise from the contribution of C···H/H···C contacts (17.5%) in the compound. The pair of wings in the fingerprint plot delineated into H···N/N···H contacts (15.8%) (Fig. 6d) are observed as a pair of spikes with the tips at $d_e + d_i$ = 2.73 Å. The fourth contribution is O···H/H···O (14.2 %) with a pair of sharp spikes at about $d_e + d_i$ = 1.18 Å, equally inclined with respect to the diagonal, indicating the presence of intermolecular C-H···O interactions, which play a role in assembling the molecules inside the crystal. The red spots over the surface direct the inter contacts tangled in the hydrogen bonds. The other minor contacts in the fingerprint plots such as C···C, C···N, C···O, N···N, O···N contacts have 2%, 1.4%, 0.4 %, 1.1% and 1.2% contributions, respectively with the tips at $d_e = d_i$ = 1.82, 3.45, 3.46, 1.7 and 3.52 Å, respectively. The 3D HS image with function of d_{norm} plotted for the all contacts, H···H, H···O/O···H, H···C/C···H and H···N/N···H interactions are shown in Fig. 7a-e, respectively.

Electrochemical studies

Electrochemical impedance spectroscopy studies: The Nyquist and Bode plots of mild steel coupons in 1 M HCl in the absence and presence of hexahydroquinoline-3-carbonitriles (**56a-f**) at 300 K are shown in Fig. 8. The Nyquist plots (Fig. 8a) shows that in the presence of quinoline-3-carbonitriles, the semicircle diameter increases compared to the blank solution, indicating improved charge-transfer resistance and reduced corrosion rate. The single peak observed in the Bode plots (Fig. 8b) suggests that the impedance data fit well with a one-time constant equivalent circuit model incorporating a constant phase element (CPE). Moreover, the higher impedance (Z) values in Fig. 8c for compounds **56a-f** compared to the blank confirm their effective corrosion inhibition. Among the synthesized hexahydroquinoline-3-carbonitriles, compound **56c** exhibited the highest inhibition efficiency of 95%.

The EIS spectra were analysed using the equivalent circuit (Fig. 1) consists of a parallel combination of the charge transfer resistance (R_{ct}), the constant phase element (CPE) and solution resistance (R_s). The EIS data (Table-2) confirmed that the value of R_{ct} increases with the addition of quinoline-3-carbonitrile derivatives as compared to the blank solution. An increase in R_{ct} value is attributed to the development of a protective film at the metal-solution interface. In addition, it shows that as the inhibitors were added in the corrosive medium C_{dl} values tend to decrease, which suggests the adsorption of inhibitor molecules at the metal-solution interface. Thus, the change in C_{dl} values was triggered *via* the gradual replace-

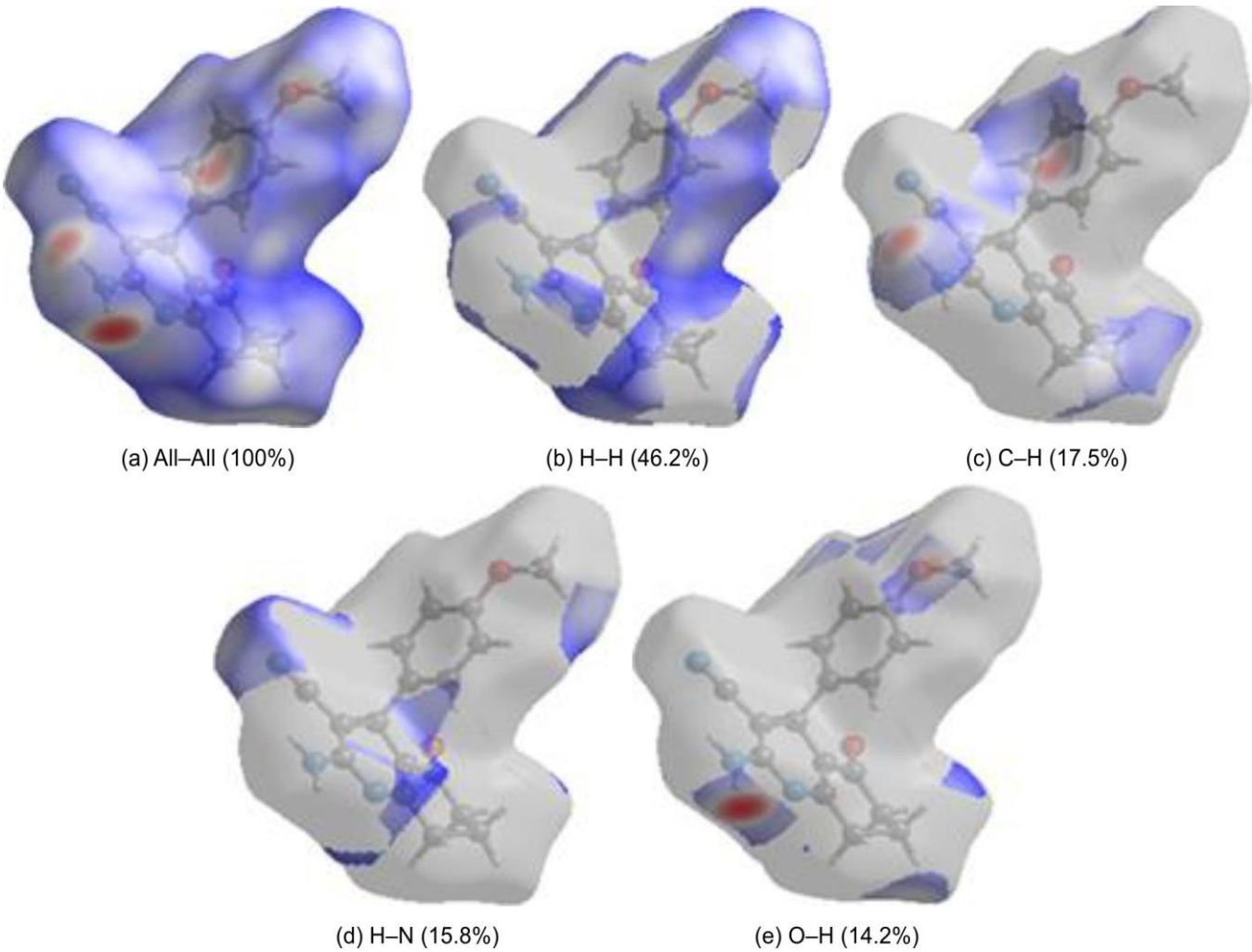

Fig. 7. Hirshfeld surface representations with the function d_{norm} plotted for intermolecular interactions of **56f**

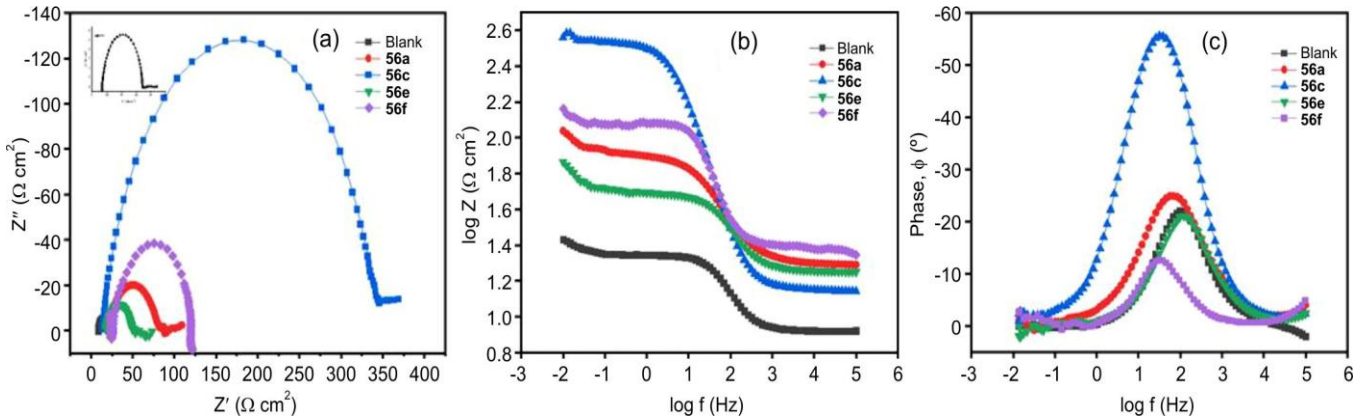

Fig. 8. Nyquist (a), Bode (b) and phase angle (c) plots of mild steel in 1 M HCl with quinoline-3-carbonitriles (**56a-f**)

TABLE-2
ELECTROCHEMICAL IMPEDANCE PARAMETER VALUES OF MILD STEEL IN 1 M HCl WITH **56a-f**

Inhibitor (M)	R_s (Ω cm²)	R_{ct} (Ω cm²)	n	Y_0 (μSn/Ω cm^{-2})	C_{dl} (μF cm^{-2})	η (%)
Blank	8.31	14.20	0.8	513.9	187.1	–
56a	21.81	89.09	0.8	315.7	129.2	84
56c	14.90	330.14	0.8	166.6	80.61	95
56e	17.76	45.34	0.8	339.7	119.67	68
56f	22.20	95.16	0.8	87.5	26.42	85

ment of water molecules through the adsorption of the organic molecules on the metal surface, lowering the extent of the metal dissolution.

Tafel polarisation studies: The Tafel polarisation curves of mild steel at optimum concentration of quinoline-3-carbonitriles (**56a-f**) are shown in Fig. 9 and indicates that the addition of quinoline derivatives reduce anodic dissolution and retard the hydrogen evolution reaction. The Tafel polarisation parameters *i.e.* corrosion potential (E_{corr}), cathodic Tafel slope (β_c), anodic Tafel slope (β_a) and corrosion current density (I_{corr}) obtained from the extrapolation of Tafel lines are given in Table-3. The polarisation curves reveal that the shifts in E_{corr} values of **56a**, **56e** and **56f** occurred towards negative direction with respect to blank.

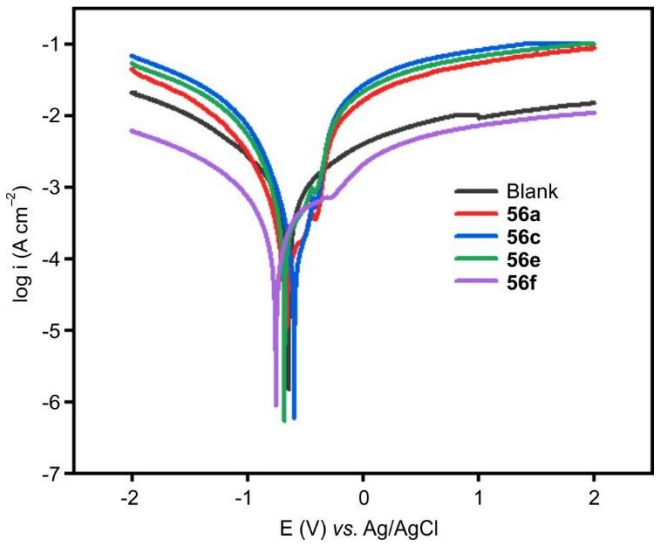

Fig. 9. Tafel polarisation curves of mild steel in 1 M HCl with quinoline-3-carbonitriles (**56a-f**)

Furthermore, the I_{corr} values are also found to be decreased in presence of quinoline-3-carbonitriles. The difference in the E_{corr} values of blank and inhibitor is less than 85 mV for **56a, 56c** and **56e**. Therefore, these compounds are mixed type inhibitors. Nevertheless, the shift in the E_{corr} value of **56f** was higher than 84 mV, so it is anodic or cathodic type. Thus, it is clear that difference between cathodic Tafel slope (β_c) and anodic Tafel slope (β_a) is not much higher than the blank solution indicating that quinoline derivatives control both cathodic and anodic inhibition. also, it shows that the mild steel surface's adsorption of quinoline derivatives lowers the rate of corrosion.

Atomic force microscopic (AFM) analysis: The AFM images of the polished and corroded mild steel surfaces in the presence and absence of quinoline derivatives were used to study the surface morphology of mild steel caused by the corrosion process. The AFM images of mild steel surface in absence and presence of inhibitor **56f** at the optimum concentrations are shown in Fig. 10a-b.

The AFM micrograph of the mild steel surface shows a highly corroded and rough surface (Fig. 10a), which was again attributed to corrosion in acid solution (blank) without any inhibitors. The calculated average surface roughness (R_a) and RMS roughness (R_q) were 211 nm, 275 nm, respectively. In contrast, the AFM image (Fig. 10b) obtained in the presence of inhibitor **56f** shows a significantly smoother metal surface, indicating the formation of a protective film by the inhibitor molecules that reduces surface corrosion. The R_a values were decreased to 118 nm in presence of 1 mM concentrations of **56f**. The R_q value of **56f** were changed to 172 nm and this decrease in surface roughness indicates that the inhibitors have adsorbed onto the mild steel surface, providing protection to the steel specimen against corrosion.

TABLE-3
TAFEL POLARISATION PARAMETERS VALUES OF MILD STEEL IN 1 M HCl WITH QUINOLINE-3-CARBONITRILES (**56a-f**)

Inhibitor (M)	$-E_{corr}$ (mV)	I_{corr} (μAcm^{-2})	β_a (mV/dec)	β_c (mV/dec)	LPR	C_r (mpy)
Blank	640.3	300.0	473.2	512.9	147	143.00
56a	680.5	234.0	473.3	674.7	162	56.03
56c	596.0	106.3	490.0	722.6	337	25.40
56e	680.0	282.5	275.6	644.5	167	67.60
56f	754.1	92.78	526.0	525.0	445	22.18

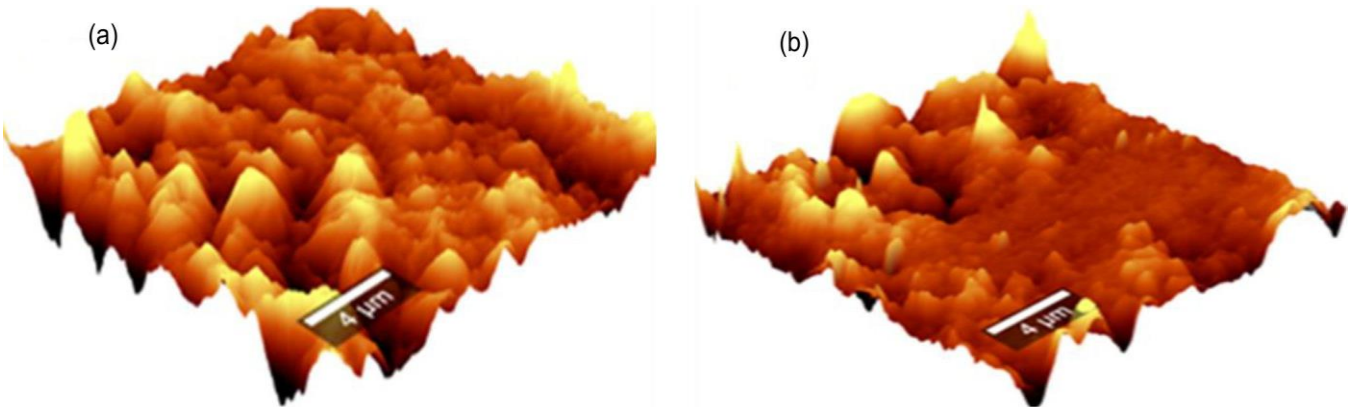

Fig. 10. AFM images of mild steel surfaces: (a) retrieved from 1 M HCl, (b) retrieved from 1 M HCl + **56f**

Mechanism of corrosion inhibition: Corrosion inhibition of metals takes place through different mechanisms such as physisorption, chemisorption and reterodonation. The adsorption process is influenced by the chemical composition of inhibitors, as well as the properties and charge of the metal surface. In the adsorption phenomenon, formation of a donor-acceptor complex between π-electrons of inhibitors and *d*-orbitals of surface metal atoms were postulated by several authors [22,23]. A corrosion inhibitor generally mitigates corrosion on mild steel through multiple mechanisms, for example, (i) it adsorbs onto the metal surface, thereby reducing the corrosion rate; (ii) It facilitates in the development of a protective film over the metal; and (iii) the inhibitor may interact with corrosive species in the environment to form a stable complex. The adsorption of the inhibitor molecules would take place through the heteroatoms such as O and N as well as π-bond.

Analysing the structure of quinoline-3-carbonitrile derivatives (**56a-f**) reveals that unshared electron pairs on heteroatoms and π-electrons in the aromatic rings contribute to chemical interaction with the mild steel surface, while the presence of diverse functional groups enhances the physical interaction. When metal undergoes rapid anodic oxidation in an acidic environment, a positive charge forms up on the metal surface, drawing chloride ions in *via* the electrostatic force of attraction. As a result, acid counter ions contribute to a negative charge on the metallic surface in an acidic environment. Furthermore, heteroatoms such as N, O, P and S undergo protonation under acidic conditions, leading to the protonated forms of heterocyclic inhibitors in such a medium. The quinoline derivatives adsorb at the metal–acid interface through multiple mechanisms, as illustrated in Fig. 11. These include: (i) electrostatic attraction between protonated inhibitor molecules and pre-adsorbed chloride ions on the metal surface

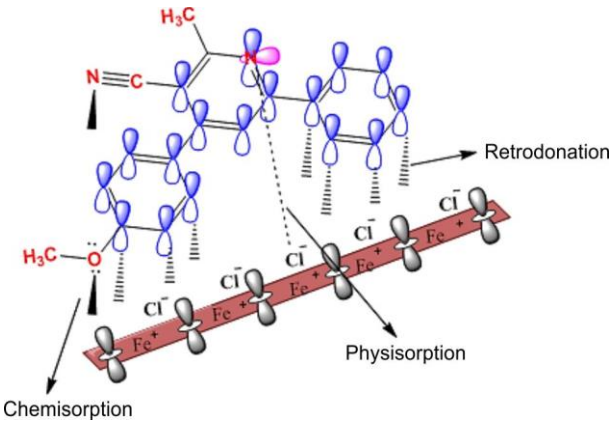

Fig. 11. Schematic illustration of the inhibitor adsorption mechanism on the mild steel

(physisorption), (ii) donor–acceptor interactions between the π-electrons of the aromatic ring or lone pairs on heteroatoms (N, O) and the vacant *d*-orbitals of iron atoms, leading to chemisorption and formation of a protective hydrophobic film, and (iii) possible back-donation from the *d*-orbitals of iron to the vacant orbitals of the inhibitor molecules (retrodonation).

Conclusion

Most of the synthesised quinoline-3-carbonitriles (**56a-f**) show excellent inhibition property for the corrosion of mild steel in 1 M HCl at 300 ± 2 K. The results of EIS indicate that the addition of inhibitors decreases the C_{dl} values and increase both R_{ct} and η% compared to the blank acid solution. As the inhibitor concentration increased, the corrosion rate of mild steel decreased. This outcome can be attributed to an increase of the thickness of the protective coating that developed on the mild steel surface which was further confirmed

from the AFM analysis. The results acquired from electrochemical impedance spectroscopy methods and potentiodynamic polarisation curves showed a reasonably high agreement. The values of metal loss and inhibition efficiencies of all the compounds were found to depend on their molecular structure. According to the results of the Tafel and EIS tests, the quinoline derivatives under investigation are effective at preventing mild steel from corroding in 1 M HCl. Moreover, it also indicates that the majority of them are mixed-type inhibitors.

Supplementary files: CCDC No. 1910687 contain the supplementary crystallographic data for this paper. These data can be obtained free of charge from the Cambridge Crystallographic Data Centre *via* www.ccdc.cam.ac.uk/data_request/cif through email: data_request@ccdc.cam.ac.uk or by contacting the Cambridge Crystallographic Data Centre, 12 Union Road, Cambridge CB2 1EZ, UK; fax: +44 1223 336033.

CONFLICT OF INTEREST

The authors declare that there is no conflict of interests regarding the publication of this article.

DECLARATION OF AI-ASSISTED TECHNOLOGIES

During the preparation of this manuscript, the authors used an AI-assisted tool(s) to improve the language. The authors reviewed and edited the content and take full responsibility for the published work.

REFERENCES

1. A. Rezvanian, Z. Saeedi and F. Bayat, *J. Mol. Struct.*, **1359**, 145314 (2026); https://doi.org/10. 1016/j.molstruc.2026.145314
2. Rajni, V. Versha, L. Singh, R. Rana and A. Bendi, *ChemistrySelect*, **7**, e202203648 (2022); https://doi.org/10.1002/slct.202203648
3. C.G. Bangcuyo, J.M. Ellsworth, U. Evans, M.L. Myrick and U.H.F. Bunz, *Macromolecules*, **36**, 546 (2003); https://doi.org/10.1021/ma0257200
4. S.A. Jenekhe, L. Lu and M.M. Alam, *Macromolecules*, **34**, 7315 (2001); https://doi.org/10.1021/ma0100448
5. A.P. Damant, Food Colourants, Woodhead Publishing Ltd. (2011).
6. N. Yilmaz, A. Fitoz, Ü. Ergun and K.C. Emregül, *Corros. Sci.*, **111**, 110 (2016); https://doi.org/10.1016/j.corsci.2016.05.002
7. G. Schmitt, *Br. Corros. J.*, **19**, 165 (1984); https://doi.org/10.1179/000705984798273100
8. H.M.H. Farh, M.E.B. Seghier and T. Zayed, *Eng. Fail. Anal.*, **143**A, 106885 (2023); https://doi.org/10.1016/j.engfailanal.2022.106885
9. H.S. Aljibori, A. Alamiery and A.A.H. Kadhum, *Int. J. Corros. Scale Inhib.*, **12**, 1476 (2023); https://doi.org/10.17675/2305-6894-2023-12-4-6
10. D.-I. Răuţă, E. Matei and S.-M. Avramescu, *Technologies*, **13**, 103 (2025); https://doi.org/10.3390/technologies13030103
11. M.A. Ahmed, S. Amin and A.A. Mohamed, *RSC Adv.*, **14**, 31877 (2024); https://doi.org/10.1039/D4RA05662K
12. H. Bairagi, P. Vashishth, G. Ji, S.K. Shukla, E.E. Ebenso and B. Mangla, *Corros. Commun.*, **15**, 79 (2024); https://doi.org/10.1016/j.corcom.2023.10.006
13. I.A. Wonnie Ma, Sh. Ammar, S.S.A. Kumar, K. Ramesh and S. Ramesh, *J. Coat. Technol. Res.*, **19**, 241 (2022); https://doi.org/10.1007/s11998-021-00547-0
14. M.A. Quraishi and D. Jamal, *Corrosion*, **56**, 983 (2000); https://doi.org/10.5006/1.3294388
15. M. Finšgar and J. Jackson, *Corros. Sci.*, **86**, 17 (2014); https://doi.org/10.1016/j.corsci.2014.04.044
16. K.R. Ansari, M.A. Quraishi and A. Singh, *Measurement*, **76**, 136 (2015); https://doi.org/10.1016/j.measurement.2015.08.028
17. S.A. Abd El-Maksoud and A.S. Fouda, *Mater. Chem. Phys.*, **93**, 84 (2005); https://doi.org/10.1016/j.matchemphys.2005.02.020
18. R. Yıldız, *Corros. Sci.*, **90**, 544 (2015); https://doi.org/10.1016/j.corsci.2014.10.047
19. D. Cremer and J.A. Pople, *J. Am. Chem. Soc.*, **97**, 1354 (1975); https://doi.org/10.1021/ja00839a011
20. J. Bernstein, R.E. Davis, L. Shimoni and N.L. Chang, *Angew. Chem. Int. Ed. Engl.*, **34**, 1555 (1995); https://doi.org/10.1002/anie.199515551
21. C.F. Mackenzie, P.R. Spackman, D. Jayatilaka and M.A. Spackman, *IUCrJ*, **4**, 575 (2017); https://doi.org/10.1107/S205225251700848X
22. B. El Mehdi, B. Mernari, M. Traisnel, F. Bentiss and M. Lagrenée, *Mater. Chem. Phys.*, **77**, 489 (2003); https://doi.org/10.1016/S0254-0584(02)00085-8
23. X. Tang, M. Li, L. Li, G.N. Mu and G.H. Liu, *Surf. Coat. Tech.*, **201**, 384 (2006); https://doi.org/10.1016/j.surfcoat.2005.11.132